ELSEVIER

Contents lists available at ScienceDirect

Biosensors and Bioelectronics

journal homepage: www.elsevier.com/locate/bios



Wearable smart textile band for continuous equine health monitoring

Taewoong Park ^a, Seokkyoon Hong ^a, Laura Murray ^b, Junsang Lee ^a, Ankit Shah ^{a,c}, Juan C. Mesa ^{a,c}, Hyowon Lee ^{a,c}, Laurent Couetil ^{b,*}, Chi Hwan Lee ^{a,c,d,e,f,g,**}

- ^a Weldon School of Biomedical Engineering, Purdue University, West Lafayette, IN, 47907, USA
- ^b Department of Veterinary Clinical Sciences, Purdue University, West Lafayette, IN, 47907, USA
- ^c Center for Implantable Devices, Purdue University, West Lafayette, IN, 47907, USA
- d Elmore Family School of Electrical and Computer Engineering, Purdue University, West Lafayette, IN, 47907, USA
- ^e School of Mechanical Engineering, Purdue University, West Lafayette, IN, 47907, USA
- f School of Materials Engineering, Purdue University, West Lafayette, IN, 47907, USA
- g Department of Speech, Language, and Hearing Sciences, Purdue University, West Lafayette, IN, 47907, USA

ARTICLE INFO

Keywords: Wearable sensors Smart textile band Equine health monitoring Asthma early diagnosis Continuous physiological monitoring

ABSTRACT

Continuous physiological monitoring is well-established in human healthcare for early disease detection and management. However, translation of these technologies to large animals such as equines remains underdeveloped due to anatomical constraints, dense hair coat coverage, and requirements for unimpeded mobility. Equines, particularly racehorses, are prone to asthma and cardiovascular abnormalities, with nearly 80 % affected by mild to moderate asthma, impacting performance and long-term health. Despite the need for continuous monitoring, existing solutions require shaving hairs, often lack wireless functionality, and are impractical for long-term use, making real-world implementation challenging. Here, we introduce a noninvasive, wireless, and adjustable smart textile band specifically designed for equines, capable of continuous monitoring of respiratory activity, cardiac function, and movement without hair removal or behavioral restriction. This work fills a critical gap in equine health monitoring by translating established sensing modalities into a practical, long-term, and field-deployable platform. The device integrates multiple sensors within a flexible, size-adjustable textile structure, ensuring compatibility across equine body types. In vivo validations confirmed its accuracy and reliability across healthy and asthmatic equines, demonstrating versatile physiological monitoring. This innovation offers a scalable solution for veterinarians, trainers, and researchers, enabling real-time monitoring in clinical and field settings.

1. Introduction

Monitoring physiological health in large animals such as horses is as critical as it is in humans but often receives less attention (Gerber et al., 2003; Chang et al., 2022). For instance, equine athletes, particularly racehorses, are highly susceptible to upper airway obstruction and asthma, with nearly 80 % experiencing mild to moderate asthma (Ivester et al., 2018; Leduc et al., 2024), and 14 % of adult horses in the general population are also affected (Hotchkiss et al., 2010), impacting both performance and well-being. These respiratory conditions can diminish athletic capability, increase veterinary costs, and even lead to career-ending health issues (Couetil et al., 2020). Cardiac diseases are

less prevalent but can also impair performance (Leroux et al., 2013). Since cardiovascular and respiratory functions are closely linked, changes in activity levels may also indicate stress, fatigue, or underlying illness (Decloedt et al., 2017; Mitchell et al., 2021).

Despite the need for continuous monitoring in equines, effective tools remain scarce. Periodic clinical assessments often fail to detect transient abnormalities or early-stage diseases, while subjective observations by trainers and veterinarians can be inconsistent, leading to delayed diagnoses (Navas de Solis et al., 2022). Traditional monitoring methods, such as auscultation, electrocardiography (ECG), respiratory endoscopy, or pulmonary function testing require restraining the animal, which induces stress and compromises measurement accuracy

^{*} Corresponding author.

^{**} Corresponding author. Weldon School of Biomedical Engineering, Purdue University, West Lafayette, IN, 47907, USA. *E-mail addresses*: couetill@purdue.edu (L. Couetil), lee2270@purdue.edu (C.H. Lee).

(Mitchell et al., 2020; Hawkins et al., 2014). Moreover, existing veterinary monitoring solutions are often designed for short-term clinical use rather than long-term, real-world applications, further limiting their effectiveness (Couetil et al., 2020; Navas de Solis et al., 2022; Mitchell et al., 2020; Kee et al., 2023).

A non-invasive, wireless, and continuous monitoring system is essential for early detection, timely intervention, and improved health outcomes in equines (Chung et al., 2020; Kwak et al., 2021; Xu et al., 2022). Real-time tracking provides a comprehensive assessment of physiological function, particularly for performance animals like racehorses, whose well-being depends on optimal respiratory and cardiovascular health (Bayly et al., 2024; Navas de Solis, 2019; Navas de Solis et al., 2024). However, many existing solutions require shaving hair for sensor attachment, making them inconvenient and unsuitable for long-term use on equines (Kim et al., 2023; Min et al., 2023; Ray et al., 2019; Wang et al., 2018; Hu et al., 2023). Additionally, clinical monitoring devices used in large animal applications often lack wireless functionality, portability, and robustness, limiting their suitability for continuous monitoring in dynamic settings (Couetil et al., 2020; Navas de Solis et al., 2022; Mitchell et al., 2020; Kee et al., 2023). Monitoring physiological signals during movement is further complicated by motion artifacts, which can obscure signal fidelity, as highlighted in recent studies (Yin et al., 2024; Fang et al., 2021; Meng et al., 2024). Addressing these limitations requires careful consideration of material selection, mechanical design, sensor placement, and signal processing strategies to ensure reliable measurements during locomotion. These challenges underscore the need for a practical, adaptable, and stress-free monitoring solution that can seamlessly integrate into equine care, enabling long-term health management without disrupting natural behavior.

To address these challenges, we developed a non-invasive, wireless, and size-adjustable smart textile band that is hair-coat-tolerant and field-compatible, providing continuous monitoring in equines where previous systems have remained impractical. Unlike conventional systems, the device accommodates any hair coat lengths and body sizes, enhancing ease of use and animal comfort without compromising signal fidelity. Comparative in vivo studies in both healthy (16-year-old Standardbred) and asthmatic (18-year-old Tennessee Walker) equines, benchmarked against gold-standard respiratory and ECG devices, confirmed the system's accuracy and robustness across multiple physiological domains. This platform enables real-time detection of subclinical abnormalities and subtle physiological changes, supporting early diagnosis, timely intervention, and personalized treatment strategies for conditions such as equine asthma, and exercise-induced cardiac arrhythmias. In equine health monitoring, it is critical not only to detect early signs of asthma before exacerbation but also to comprehensively track recovery during treatment, as inadequate information can lead to worsening airway obstruction (Petsche et al., 1994). Leveraging mechano-acoustic sensing, our device uniquely employs only an accelerometer to capture both respiration and heart rate by detecting subtle local vibrations from breathing and heartbeat, without interference from global body movements. This approach eliminates the need to shave fur and enables easy, continuous, and long-term monitoring, while its high-resolution data acquisition and field-deployable design provide veterinarians, trainers, and researchers with a powerful tool for longitudinal health monitoring that bridges the gap between traditional clinical assessments and real-world equine healthcare.

2. Materials and methods

2.1. Electronic system design and fabrication

Schematic diagrams and layouts for a flexible printed circuit board (fPCB) were generated using commercial software (Autodesk Eagle Version 9.6.2). The smart textile band was designed with a three-layer stacked, three-island fPCB, integrating commercially available

electronic components. The first island housed a three-axis digital accelerometer, a custom-designed ECG amplifier, and a microphone. The second island contained the battery charging and voltage regulator circuits, while the third island housed a Bluetooth Low-Energy (BLE) system-on-chip (SoC) and LEDs. Customized firmware was uploaded to the BLE SoC. Surface-mount components were soldered onto the fPCB using solder paste (SMDLTLFP10T5, Chip Quik), a heat gun (Int866, Aqyue), and a hot plate (MHP30, Miniware). A commercial textile band (Magnetic Urban Elastic Belt, Xpand) was integrated between the first and second layers of the fPCB. The entire structure was then encapsulated with a soft, waterproof elastomer (Ecoflex 00–35, Smooth-On) to protect against external factors, ensuring durability and flexibility.

2.2. Validation devices

The components of the flow and microphone sensor, used for the validation of respiratory signals in conjunction with clinical equipment, include a thermal gas flow sensor (FS7, Innovation Sensor Technology), a waterproof microphone (MW042502-1, DB Unlimited), and a BLE SoC (nRF52840, Nordic Semiconductor). Additionally, for comprehensive and time-synchronized analysis, we employed a custom-designed ECG amplifier as the gold standard for heart rate (HR) measurement, featuring a bandwidth of 0.5–40 Hz and a gain of 1000.

2.3. Encapsulation process

A mold was designed using commercial 3D CAD software (Autodesk Fusion 360 Version 2.0) and fabricated with a stereolithography 3D printer (Form3, Formlabs). Prior to encapsulation, a silicone release agent (Ease Release 200, Mann Release Technologies) was applied. The sensor module and textile band were then placed inside the mold, and encapsulation was carried out using a soft elastomer gel (Ecoflex 00–35, Smooth-On) to ensure waterproofing and mechanical resilience.

2.4. Mechanical analysis

Finite Element Analysis (FEA) was conducted using Abaqus to investigate the stress and strain distribution within the sensor module subjected to stretching and twisting. The model comprised a polyimide (PI) frame embedded in an Ecoflex 00–35 matrix, incorporating an integrated textile component. Linear elastic material properties was assigned to the PI frame, with elastic moduli of 7.1 GPa, and Poisson's ratios of 0.30, while the Ecoflex 00–35 body was modeled using a Neo-Hookean hyperelastic model, with material coefficients $\rm C10=0.0113$ and $\rm D1=1.96$. The textile material was characterized using an Ogden hyperelastic model, derived from uniaxial tensile testing data. Boundary conditions were applied to the edges of the textile component. For experimental validation, a motorized force tester (ESM303, Mark-10) was used to subject the smart textile band to controlled stretching conditions, verifying its mechanical performance.

2.5. Comprehensive benchtop tests

The vibrational response of the sensor module was analyzed using a vibration generator (1000701, 3B Scientific) and an arbitrary waveform generator (3390, Keithley). Targeted vibration waveforms were applied at 0.13 Hz, 0.27 Hz, 0.47 Hz, and 0.67 Hz, using a square wave at 10 V peak-to-peak with an 80 % duty cycle. To assess sweat resistance, the sensor module was repeatedly exposed to 0.9 % saline solution (37–6240, McKesson) for 15 s intervals. The device maintained normal functionality under continuous saline flow, successfully transmitting sensor data via Bluetooth without signal degradation.

2.6. Sensor data analysis

All signal processing was performed using MATLAB (R2024a,

MathWorks). The raw respiration and cardiac signals were analyzed over a continuous recording period. To enable localized analysis of respiratory rate (RR) and HR, the signal was divided into consecutive, non-overlapping 20 s windows. Each segment was independently processed to estimate RR and HR based on the dominant physiological components. To isolate the respiratory and cardiac dynamics, a Continuous Wavelet Transform (CWT) was applied to each segment using the analytic Morlet ("amor") wavelet. For RR, wavelet coefficients corresponding to frequencies below 0.5 Hz were extracted to capture typical equine breathing patterns. For HR, coefficients between 5 Hz and 15 Hz were selected to target the dominant frequency content associated with heartbeat activity. The relevant coefficients were summed across their respective frequency ranges to reconstruct time-domain signals enriched in respiratory or cardiac activity. The reconstructed signals were mean-centered and normalized to unit amplitude. Valleys in the waveform—corresponding to respiratory or heartbeat cycles—were identified using MATLAB's "findpeaks" function. A dynamic threshold was applied to minimize false detections. RR and HR were then calculated for each segment based on the average interval between successive valleys. Specifically, the interval between detected valleys was computed and converted to BPM using the equation:

Respiration and Heart Rate (BPM) =
$$60/\text{Average Interval (s)}$$
 (1)

Spectrogram analysis was conducted using the 'spectrum' function to visualize frequency distribution over time, while fast Fourier transform (FFT) analysis was performed using the 'FFT' function to identify periodic signal components and gain deeper insights into signal characteristics.

2.7. SNR calculation

Signal-to-noise ratio (SNR) was calculated using power spectral density estimation in MATLAB. The SNR in decibels (dB) was determined using the equation:

$$SNR_{dB} = 10 \log_{10} (P_{\text{signal}} / P_{\text{noise}})$$
(2)

where P_{signal} represents the power of the signal and P_{noise} represents the power of the noise.

2.8. Treadmill exercise test

The Purdue Animal Care and Use Committee approved this protocol (#1111000176). A 16-year-old Standardbred mare owned by Purdue University was used in the treadmill study. The horse had been previously trained to exercise on the high-speed treadmill (High Speed Treadmills, EquiGym) and was physically fit. On the day of testing, the horse was equipped with a smart textile band tightly adjusted around the chest with the electronic device placed against the chest at the level of the point of the elbow on the left side. The haircoat was clipped over 3 areas (5 × 5 cm) and ECG electrodes (MDSM611550, Medline) glued to the skin over conducting gel. A surcingle was positioned immediately caudal to the smart textile band that was equipped with a dorsal hook to secure the safety belt once on the treadmill. The abdominal band was placed tightly around the caudal flank region with the electronic device positioned over the external abdominal oblique muscles on the left side. Then, a fiberglass facemask was placed over the horse's nose, secured to the bridle and two ultrasonic phase-shift flowmeters (FR-41eq, Flowmetrics) were fitted to measure airflow from each nostril. Output signals from the flowmeters were recorded by computer software (Pulmonary mechanics analyzer, Buxco Electronics). Each flowmeter was calibrated prior to the experiment up to 60 l/s using a rotameter system. The thermal gas flow sensor and waterproof microphone were affixed in front of the ultrasonic flowmeter over the right nostril of the horse. Once fitted with the monitoring equipment, the horse was walked onto the treadmill, secured to the safety belt, and exercise protocol initiated. The

exercise test consisted of walking at 1.5 m/s on the flat for 15 min, followed by trotting at 4.5 m/s for 30 min, and walking at 1.5 m/s for 6 min. The treadmill exercise test was conducted under veterinary supervision, with continuous assessment of gait, posture, and behavior to ensure animal comfort and safety (Gleerup et al., 2015; De Grauw et al., 2016).

2.9. Pulmonary function testing in a horse with acute asthma

The Purdue Animal Care and Use Committee approved this protocol (#1111000176). An 18-year-old Tennessee Walker mare presented for acute exacerbation of asthma. The mare had a history of severe asthma exacerbation that was reversible with appropriate therapy and low-dust diet. The evaluation was performed in a temperature-controlled room maintained at 20 °C while the horse was restrained in stocks. An esophageal balloon catheter was passed through the nose, advanced to mid-thorax and connected to a pressure transducer (DP45-30, Validyne Engineering) on one side with the other side connected to the facemask to measure transpulmonary pressure as previously described (Couëtil et al., 2001). A pneumotachometer (#4 Fleisch, EMKA Technologies) was positioned on the facemask fitted over the horse's muzzle and connected to a differential pressure transducer (DP-/45-14, Validyne Engineering) via two identical Teflon catheters to measure airflow. The output signals from the pressure transducers were continuously recorded using a software (Pulmonary Mechanics Analyzer -XA version, Buxco Electronics).

Resistance (RL) was measured using the isovolume 50 % method. Dynamic compliance (Cdyn) was computed by dividing tidal volume by the difference in Δ PLmax between points of zero flow. Other parameters measured breath-by-breath included respiratory rate, tidal volume, inspiratory time, expiratory time, peak inspiratory flow, peak expiratory flow, and minute ventilation. Pulmonary function was measured at baseline over approximately 12 min and the average data from breaths without artifacts (e.g. swallowing) was used for analysis. Then, the horse was given an anticholinergic bronchodilator (N-butylscopolamonium bromide, Buscopan injectable solution, 0.3 mg/kg IV, Boehringer Ingelheim) and pulmonary function testing was repeated 10 min later. Data recorded over the following 3 min were averaged after eliminating breaths with artifacts. Pulmonary function testing in the asthmatic horse was performed under veterinary supervision, with careful monitoring of respiratory effort, gait, and behavioral cues to confirm tolerance of the procedure (Gleerup et al., 2015; De Grauw et al., 2016).

3. Results

3.1. Overall system design and benchtop evaluation

Fig. 1A presents the smart textile band, designed for continuous monitoring of respiratory activity, cardiac function, and movement while maintaining wireless connectivity positioned on the chest and abdomen (Fig. S1A). The internal sensor module is built on the fPCB integrating 32 active and passive components for comprehensive data acquisition and processing. Key system components include: (1) Ultralow noise MEMS microphone (ICS-40720, TDK InvenSense); (2) Three-axis digital accelerometer, three-axis digital gyroscope, and thermometer (BMI 160, Bosch); and (3) BLE SoC (nRF52840, Nordic Semiconductor). The full layout of the fPCB and detailed schematic of the electronic subsystems are illustrated in Fig. S1B. The system enables wireless data transmission using BLE protocols. It supports over 15 h of battery life before requiring a recharge, with an average current consumption of 9.82 mA and a 150 mAh battery capacity.

The internal sensor module is linked by serpentine interconnectors and encased in a three-layer structure, shielded with a soft, waterproof elastomer to enhance durability, resist sweat, and maximize skin comfort (Fig. 1B and C). The textile band, compatible with various fabric materials, is positioned between the first and second layers of the fPCB

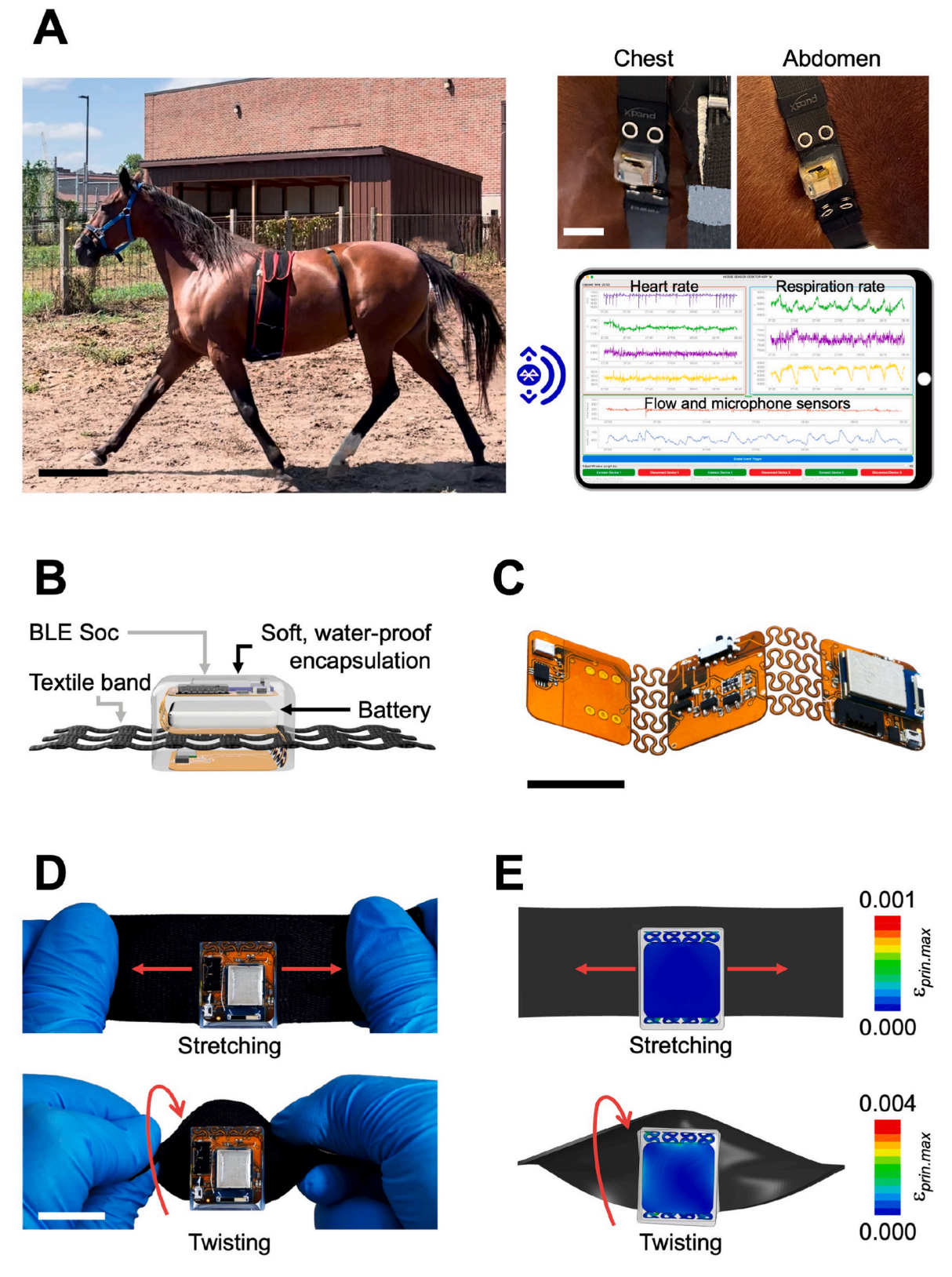


Fig. 1. Overall system design for equine physiological monitoring with enhanced wearability. (A) Schematic illustration of the smart textile band applied to a horse (scale bar, 20 cm). Insets show close-up images of the sensor-embedded textile band and secure attachment mechanism on the horse's chest and abdomen (top right; scale bar, 2 cm), along with example data visualization of physiological signals transmitted wirelessly (bottom right). (B) Exploded view and layout of the flexible electronic device. (C) Image of the unfolded layout of the flexible electronic circuit (scale bar, 2 cm). (D) Images of the smart textile band under mechanical deformation, including stretching (top) and twisting with 10 % stretching (bottom) (scale bar, 2 cm). (E) Corresponding strain distribution maps obtained through FEA under 10 % stretching (top) and twisting with 10 % stretching (bottom). FEA: Finite Element Analysis.

(Fig. S1C). Designed for flexibility, it can stretch and twist freely, ensuring improved comfort and usability (Fig. 1D). The FEA results shown in Fig. 1E indicate that the folded, three-layer sensor module experiences a maximum principal strain of less than 1 % under conditions of 10 % stretching and simultaneous twisting (Marlin et al., 2002). By integrating soft packaging with an adjustable, stretchable textile

band, the system ensures long-term wearability with a secure and comfortable fit, even during dynamic activities.

The practical performance of the smart textile band was evaluated through comprehensive benchtop tests, assessing its response to external vibrations, stretching, and saline exposure (Park et al., 2024). Vibration evaluation focused on typical equine RR and HR frequency bands:

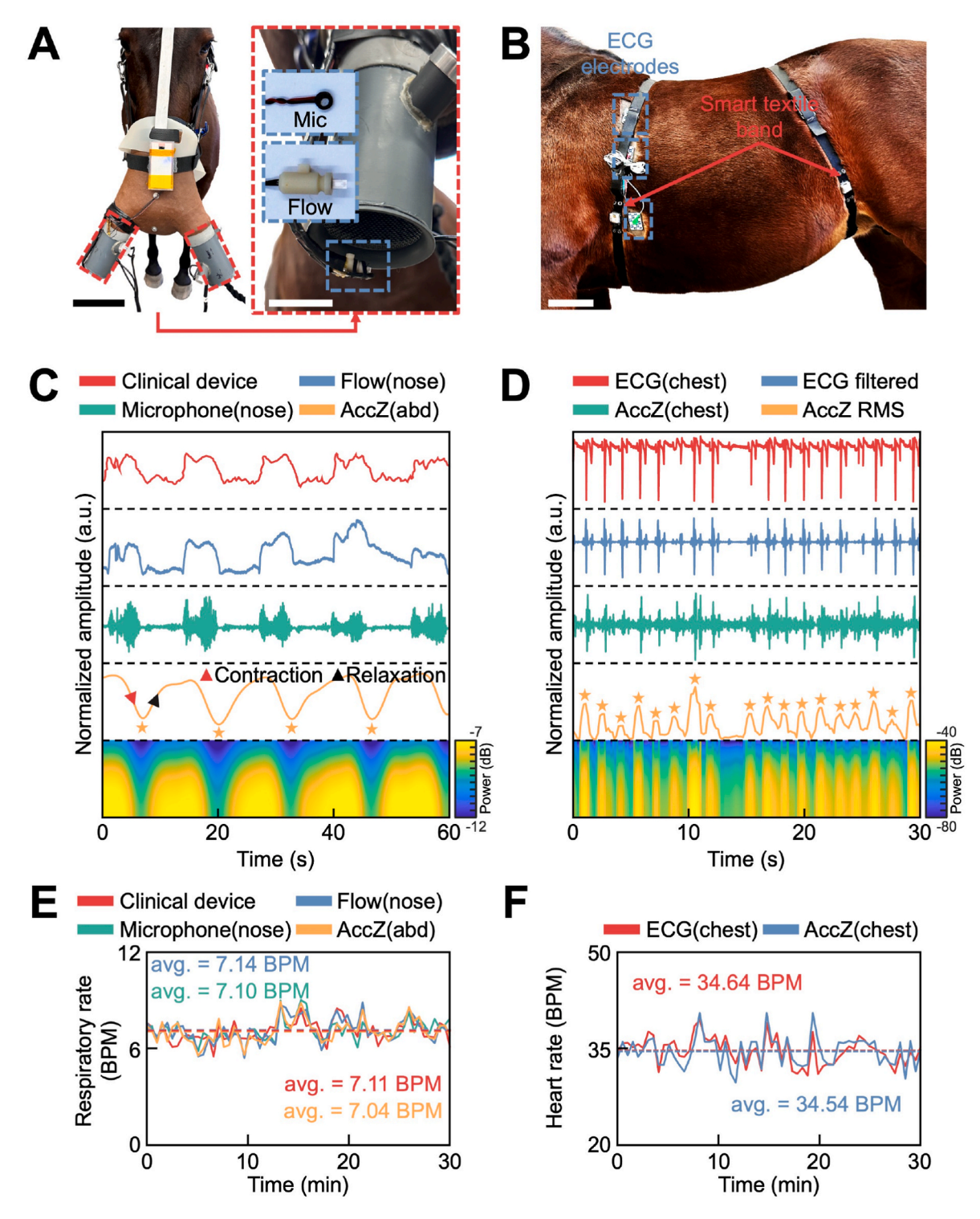


Fig. 2. Validation of equine respiration and cardiac activity monitoring. (A) Schematic and photographic images of the clinical respiratory monitoring setup alongside the developed wireless respiratory sensor system (scale bar, 10 cm). The inset shows a detailed view of the flow sensor and microphone embedded within the equine mask for respiratory signal acquisition (scale bar, 2.5 cm). (B) Smart textile band system for simultaneous monitoring of cardiac and respiratory activity (scale bar, 10 cm). (C) Representative respiratory signals measured during in vivo validation. (D) Simultaneously recorded cardiac signal during in vivo validation. (E) Continuous monitoring of respiration rate over 30 min period.

0.13–0.27 Hz for RR and 0.47–0.67 Hz for HR (Scott et al., 2020). Fig. S2A shows the SNR results for RR frequencies, with 39.36 dB at 0.13 Hz and 36.32 dB at 0.27 Hz. Similarly, Fig. S2B reports 35.73 dB at 0.47 Hz and 39.55 dB at 0.67 Hz, confirming the system's ability to capture clear signals in these targeted frequency ranges.

Further FFT analysis (Fig. S2C) reveals distinct signal peaks at 0.13 Hz, 0.27 Hz, 0.47 Hz, and 0.67 Hz, demonstrating the system's precision in detecting physiological signals. Fig. S3 presents the mechanical evaluation of the device-embedded textile and bare textile under 10 % stretch (Chang et al., 2023; Lee et al., 2020). The elastic modulus of the smart textile band measured 913 kPa, compared to 689 kPa for the bare textile. The band sustained up to 140 % strain before breaking, showcasing its resilience.

To assess environmental durability, saline solution tests were conducted following established methodologies. As shown in Fig. S4, the device maintained full functionality under continuous saline flow, demonstrating robustness in conditions simulating prolonged usage and intense physical activity. These results confirm the smart textile band's reliability for real-world applications, where movement and perspiration pose common challenges in continuous physiological monitoring.

3.2. Analysis of respiratory and cardiac signals

Fig. 2A presents images of the clinical equipment used for equine respiratory measurements (red dotted box), alongside our developed wireless respiratory sensor system, which integrates a microphone and flow sensor (blue dotted box) (Fig. S5). Fig. 2B shows the smart textile band positioned on the chest and abdomen for HR and RR measurements. To compare respiratory measurements, data were collected from clinical equipment, the flow sensor, and microphone positioned in front of the nose, while the smart textile band was placed on the abdomen. Fig. 2C illustrates respiratory signals recorded from four different sensors: the clinical equipment, the flow sensor, microphone, and the Z-axis data from the three-axis accelerometer, along with the spectrogram of the Z-axis acceleration.

For cardiac signal monitoring, we used ECG signals solely as a reference standard to validate our system. Specifically, the ECG served as the gold standard for heart activity monitoring, against which we compared the Z-axis acceleration signals acquired from the smart textile band placed on the chest. A modified version of the smart textile band was used for this analysis, integrating an ECG amplifier, a three-axis accelerometer, a temperature sensor, and a microphone (Fig. S6A and S6B). The ECG electrodes were attached to specific anatomical locations using a three-electrode configuration, as shown in Fig. S6C (Lorello et al., 2019; Mitchell, 2019; Verheyen et al., 2010). Fig. 2D presents HR measurements derived from ECG, a 5-15 Hz band-pass filtered signal, Z-axis acceleration, root-mean square (RMS) values of the Z-axis acceleration, and the spectrogram of the Z-axis acceleration. The chest Z-axis acceleration signal used for heart rate measurement demonstrated an SNR of 14.34 dB, which represents a sufficiently effective condition for reliable peak detection of biosignals (Kim, H. et al., 2010; Vadrevu, S. et al., 2019).

Fig. 2E shows continuous respiratory rate measurements over 30 min at rest, recorded using clinical equipment, the flow sensor, the microphone, and the Z-axis acceleration. The average RR values were 7.11 BPM (clinical equipment), 7.14 BPM (flow sensor), 7.10 BPM (microphone), and 7.04 BPM (Z-axis acceleration). Fig. 2F presents HR measurements over the same period, with the ECG recording an average HR of 34.64 BPM and the Z-axis acceleration recording 34.54 BPM. To further assess measurement accuracy, Fig. S7A displays the Bland–Altman plot for RR, showing a mean difference of 0.06 BPM and an RR deviation of 0.53 BPM. Fig. S7B presents the Bland–Altman plot for HR, with a mean difference of 0.10 BPM and an HR deviation of 1.65 BPM. These results confirm the high accuracy and reliability of our smart textile band in tracking respiratory and cardiac parameters in horses at rest.

3.3. Treadmill and free movement evaluation

Fig. 3A presents images of the experimental setup on a treadmill, showing the horse in a stationary state, walking at 1.5 m/s, and trotting at 4.5 m/s on a flat treadmill. Fig. S8A illustrates the process of securing the horse on the treadmill, while Fig. S8B shows the clinical equipment used for measuring respiration, along with the flow sensor and microphone we developed. Fig. S8C depicts the data acquisition module of the clinical system, and Fig. S9 provides an overview of real-time wireless data transmission along with flow data from the clinical equipment during the treadmill experiment.

Fig. 3B shows the physiological signals used to compare respiration measurements obtained from the smart textile band, a microphone, and a flow sensor. Respiratory data were extracted from the microphone and flow sensor positioned in front of the nose, as well as from the Z-axis acceleration recorded by the textile band placed on the abdomen. The flow sensor also captured sneezing events. Fig. 3C presents cardiac activity monitoring results. HR was derived by comparing ECG signals (used as the gold standard) with the Z-axis acceleration signals recorded by the textile band placed on the chest. The chest ECG and Z-axis acceleration signals used for heart rate measurement exhibited SNRs of 15.41 dB and 14.51 dB, respectively, which are considered sufficient for reliable peak detection of biosignals (Kim et al., 2010; Vadrevu et al., 2019). Temperature variations, body surface sound, as well as energy expenditure (EE) on the chest and abdomen were continuously monitored throughout the experiment (Fig. S10 and Movie S1). Additionally, 3D scatter plots of accelerations from the chest and abdomen are presented in Fig. S11A and S11B, respectively, enabling rapid assessment of body movement behavior characteristics.

Supplementary data related to this article can be found online at htt ps://doi.org/10.1016/j.bios.2025.118073

Fig. 3D displays the RR recorded continuously over 30 min using the clinical device, flow sensor, and Z-axis acceleration. During the initial walking state (11 min), the average RR values were 60.47 BPM (clinical equipment), 60.11 BPM (flow sensor), and 62.34 BPM (Z-axis acceleration). In the subsequent trotting state (16 min), average RR values were 110.96 BPM (clinical equipment), 110.06 BPM (flow sensor), and 110.89 BPM (Z-axis acceleration). In the final walking state (3 min), the recorded average RR values were 66.91 BPM (clinical equipment), 68.57 BPM (flow sensor), and 71.02 BPM (Z-axis acceleration). Similarly, Fig. 3E presents the HR measurement results during walking for 11 min, trotting for 16 min, and walking again for 3 min. During the initial walking phase, the average HR recorded by the ECG was 59.09 BPM, while the Z-axis acceleration recorded 58.94 BPM. During the trotting phase, the ECG recorded the average HR of 102.82 BPM, with Z-axis acceleration at 104.16 BPM. Finally, during the second walking phase, the ECG recorded the average HR of 72.73 BPM, while Z-axis acceleration measured 75.08 BPM. Bland-Altman plots for RR and HR are shown in Fig. S12, with a mean difference for RR of 1.06 BPM and a measurement deviation of 4.39 BPM. The mean difference for HR was 0.90 BPM, with a measurement deviation of 4.49 BPM.

Additionally, Fig. S13 presents images of the free movement experiment conducted outdoors. Physiological data were successfully collected under free movement conditions, allowing for quantitative comparisons of activity levels. These results confirm the system's applicability beyond controlled treadmill experiments, demonstrating its potential for real-world equine health monitoring. While ambient electromagnetic interference can affect data transmission range, reliable measurements were achieved at distances of 5–10 m and can be extended up to 120 m, with a Bluetooth bridge or mesh extender (Fig. S14 and Movie S2).

Supplementary data related to this article can be found online at htt ps://doi.org/10.1016/j.bios.2025.118073

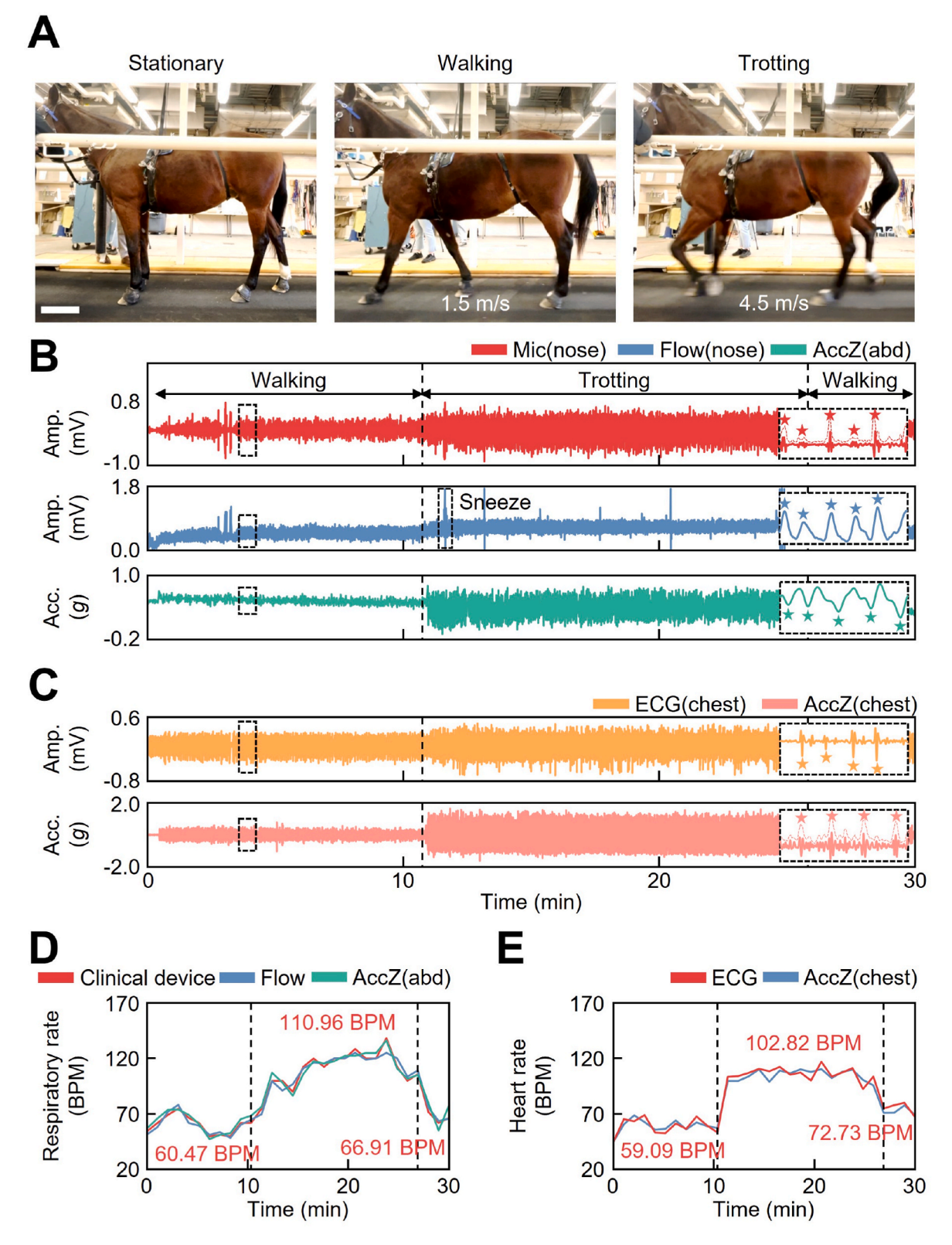


Fig. 3. Validation of physiological monitoring during treadmill experiment. (A) Photographic images of the horse during treadmill experiments (scale bar, 20 cm). (B) Representative respiratory signals measured during the treadmill exercise. (C) Simultaneously recorded cardiac signals. (D) Continuous monitoring of respiration rate throughout the treadmill exercise. (E) Continuous monitoring of heart rate during the treadmill exercise.

3.4. Physiological monitoring of asthmatic equine

Fig. 4A and S15A present the experimental setup for an asthmatic equine. This experiment used multiple measurement systems, including

an esophageal balloon catheter for pleural pressure (Fig. S15B), nasal airflow sensors (pneumotachometer and custom flow sensor), and a smart textile band. Fig. 4B illustrates the abdominal movements associated with relaxation and contraction during an asthmatic state. Fig. 4C

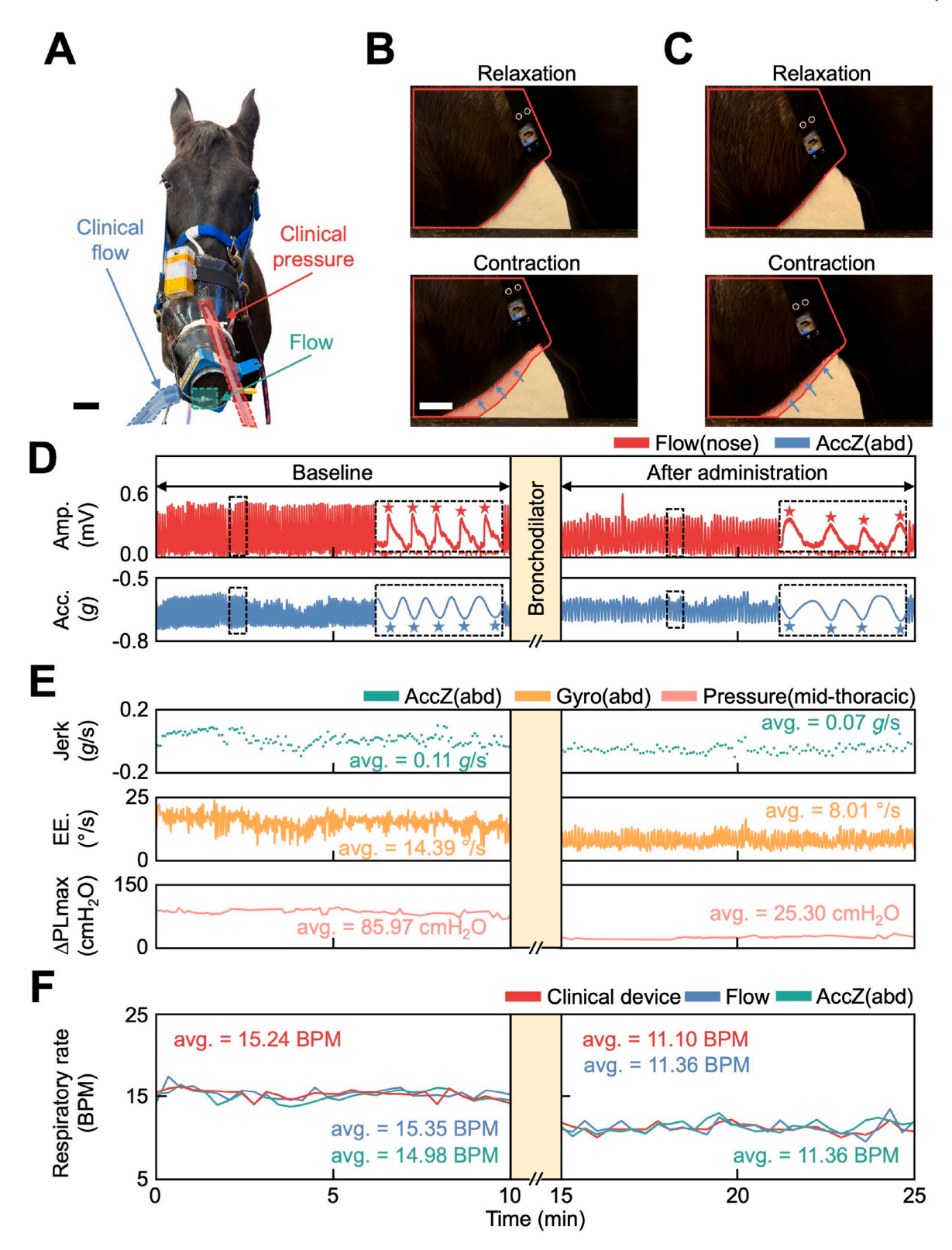


Fig. 4. Validation of respiratory monitoring in an asthmatic equine model. (A) Photographic image of the experimental setup (scale bar, 5 cm). (B and C) Abdominal movement differences associated with respiration before (B) and after (C) bronchodilator administration (scale bar, 4 cm). (D) Representative respiratory signals measured before and after bronchodilator administration. (E) Additional physiological signals measured during the experiment. (F) Continuous monitoring of respiration rate before and after bronchodilator administration.

shows the abdominal movements 5 min after intravenous administration of a bronchodilator (Buscopan injectable solution, 0.3 mg/kg IV, Boehringer Ingelheim), highlighting the changes in relaxation and contraction (Movie S3).

Supplementary data related to this article can be found online at htt ps://doi.org/10.1016/j.bios.2025.118073

Fig. 4D presents respiratory-related physiological data collected using the flow sensor and the abdominal smart textile band. Fig. 4E

compares abdominal movement intensity before and after bronchodilator administration using two indicators derived from the smart textile band-jerk (the gradient of the Z-axis acceleration graph) and EE (the RMS magnitude of the three-axis gyroscope data)-along with transpulmonary pressure measurements from the clinical equipment (Mohapatra et al., 2024). After bronchodilator administration, jerk decreased by 36 %, and EE decreased by 44 %. The mean maximum change in transpulmonary pressure decreased by 71 % (85.97 cmH₂O to 25.30 cmH₂O), consistent with previous clinical studies (Couetil et al., 2012; De Lagarde et al., 2014). Additional physiological data, including ECG and temperature variations, are provided in Fig. S16A. Continuous HR measurements over 10 min period before and after bronchodilator administration, obtained using both ECG and Z-axis acceleration data, are shown in Fig. S16B. Prior to administration, the average HR was 43.51 BPM (ECG) and 43.18 BPM (Z-axis acceleration). Following bronchodilator administration, the average HR increased to 58.27 BPM (ECG) and 58.30 BPM (Z-axis acceleration), reflecting an increase of approximately 15 BPM. This change is consistent with a previous clinical report on the physiological effects of N-butylscopolammonium bromide in asthmatic horses (De Lagarde et al., 2014; Mozo Vives et al., 2024). Fig. S17A shows the Bland–Altman plot comparing HR measurements obtained from ECG and Z-axis acceleration prior to bronchodilator administration. The mean difference was 0.33 BPM, with a measurement deviation of 1.93 BPM. Fig. S17B presents the Bland-Altman plot after bronchodilator administration, showing a mean difference of 0.04 BPM and a measurement deviation of 1.89 BPM. Comprehensive respiratory function data, including dynamic lung compliance (Cdyn), lung resistance (Rl), peak inspiratory flow (PIF), peak expiratory flow (PEF), tidal volume (TV), minute ventilation (MV), inspiratory time (Ti), and expiratory time (Te), are summarized in Fig. S18.

Fig. 4F shows continuous RR measurements over 10 min period before and after bronchodilator administration, obtained using the clinical equipment, the flow sensor, and the Z-axis acceleration. Before administration, the average RR was 15.24 BPM (clinical equipment), 15.35 BPM (flow sensor), and 14.98 BPM (Z-axis acceleration). After bronchodilator administration, the average RR decreased to 11.10 BPM (clinical equipment), 11.36 BPM (flow sensor), and 11.36 BPM (Z-axis acceleration), indicating a reduction of approximately 4 BPM that is consistent with a previous clinical report of the physiological effects of N-butylscopolammonium bromide in asthmatic horses (Couetil et al., 2012; De Lagarde et al., 2014).

Fig. S19A shows the Bland–Altman plot of RR measurements comparing the clinical flowmeter and smart textile band prior to bronchodilator administration. The mean difference in RR was 0.26 BPM, with a measurement deviation of 0.68 BPM. Fig. S19B presents the Bland–Altman plot of RR measurements after bronchodilator administration, showing a mean difference of 0.10 BPM and a measurement deviation of 0.69 BPM.

4. Conclusions

This study demonstrates the potential of a non-invasive, wireless, and adaptable smart textile band for continuous monitoring of respiratory, cardiac, and activity parameters in equines. The device provides a practical alternative to existing clinical systems, addressing key limitations such as the need for shaving hair, restricted mobility, and discomfort from rigid sensors or limited-length textile bands. Comparative in vivo studies confirmed strong agreement with gold-standard respiratory and ECG devices, as supported by Bland–Altman analysis.

The primary strength of this system lies in its versatility across diverse settings, from controlled treadmill trials to free movement scenarios. Unlike traditional equipment that restricts mobility, the wearable platform enables real-time, long-term monitoring without interfering with natural behavior—making it particularly valuable for performance animals such as racehorses. While conventional clinical instruments (e.g., esophageal balloon catheter and pneumotachometer)

provide highly precise and direct measurements of respiratory mechanics, they are invasive and unsuitable for continuous, field-based use. In contrast, our smart textile band offers a non-invasive, field-deployable solution that enables long-term, real-world monitoring of equine health, thereby enhancing both efficiency and feasibility in continuous data collection.

A key application of this technology lies in the detection and monitoring of equine asthma, a condition affecting 14 % of adult horses (Hotchkiss et al., 2010). Demonstrating the signal differences between respiration during asthma and after bronchodilator administration represents a substantial advancement in asthma detection. Furthermore, our smart textile band enables not only the detection of asthma symptoms but also the continuous monitoring of both respiration and heart rate. As the breathing strategy of asthmatic horses evolves with worsening airway obstruction (Petsche et al., 1994), wearable, non-invasive monitoring offers an opportunity for early identification of exacerbations—potentially before clinical signs are evident. Future studies will be designed to test this hypothesis and further validate the band's utility in early disease intervention.

Benchtop testing validated the sensor's robustness under mechanical stress and environmental exposure, including sweat and repeated saline immersion, indicating suitability for extended use in real-world conditions such as veterinary clinics and training environments.

Future developments may incorporate additional biosensors to measure blood oxygenation, hydration status, and cortisol levels, expanding its clinical relevance (Luo et al., 2023; Pan et al., 2024; Shirzaei Sani et al., 2023; Song et al., 2020; Wang et al., 2022). Beyond equine health, the system's adaptability suggests promise for use in other large animals, including wildlife and zoo species, broadening its impact. Moreover, integration with veterinary telemedicine platforms could enable remote, continuous health surveillance, advancing accessibility and quality of care.

In summary, this work introduces a practical, high-fidelity solution for large-animal physiological monitoring, with broader implications for both veterinary applications and the future development of human-wearable health technologies.

CRediT authorship contribution statement

Taewoong Park: Writing - review & editing, Writing - original draft, Visualization, Validation, Software, Resources, Methodology, Investigation, Formal analysis, Data curation, Conceptualization. Seokkyoon Hong: Writing - review & editing, Methodology, Investigation. Laura Murray: Writing - review & editing, Methodology, Investigation. Junsang Lee: Writing - review & editing, Visualization, Methodology, Investigation. Ankit Shah: Writing - review & editing, Methodology, Investigation. Juan C. Mesa: Writing – review & editing, Investigation. Hyowon Lee: Writing – review & editing, Investigation. Laurent Couetil: Writing – review & editing, Writing – original draft, Visualization, Validation, Supervision, Resources, Project administration, Methodology, Investigation, Funding acquisition, Formal analysis, Data curation, Conceptualization. Chi Hwan Lee: Writing - review & editing, Writing - original draft, Visualization, Validation, Supervision, Resources, Project administration, Methodology, Investigation, Funding acquisition, Formal analysis, Data curation, Conceptualization.

Funding

This work is partly supported by the National Institutes of Health (NIH) National Institute of Biomedical Imaging and Bioengineering (NIBIB) [grant number 1R21EB034879-01A1] for the design and fabrication of the wireless unit in the electronic textile device; and funding for the project was provided in part by the state of Indiana and the PVM research account funded by the total wager tax.

Declaration of competing interest

The authors declare that they have no known competing financial interests or personal relationships that could have appeared to influence the work reported in this paper.

Acknowledgements

C.H.L. acknowledges support from the Leslie A. Geddes Endowment.

Appendix A. Supplementary data

Supplementary data to this article can be found online at https://doi.org/10.1016/j.bios.2025.118073.

Data availability

The data that support the plots and other findings of this study are available from the corresponding authors upon reasonable request.

References

- Bayly, Warwick M., Leguillette, Renaud, Sides, Raymond H., Massie, Shannon, Guigand, Charline, Blythe Jones, K., Warlick, Linnea M., Thueson, Emily L., Troudt, Tristan A., Slocombe, Ronald F., Jones, James H., 2024. Equine exerciseinduced pulmonary hemorrhage: the role of high left-heart pressures secondary to exercise-induced hypervolemia, and high inspiratory pressures. J. Appl. Physiol. 137, 1359–1373. https://doi.org/10.1152/japplphysiol.00575.2023.
 Chang, Taehoo, Akin, Semih, Kim, Min Ku, Murray, Laura, Kim, Bongjoong,
- Chang, Taehoo, Akin, Semih, Kim, Min Ku, Murray, Laura, Kim, Bongjoong, Cho, Seungse, Huh, Sena, Teke, Sengul, Couetil, Laurent, Byung-Guk Jun, Martin, Lee, Chi Hwan, 2022. A programmable dual-regime spray for large-scale and custom-designed electronic textiles. Adv. Mater. 34, e2108021. https://doi.org/ 10.1002/adma.202108021.
- Chang, Taehoo, Akin, Semih, Cho, Seungse, Lee, Junsang, Lee, Seul Ah, Park, Taewoong, Hong, Seokkyoon, Yu, Tianhao, Ji, Yuhyun, Yi, Jonghun, Gong, Sunland L., Kim, Dong Rip, Kim, Young L., Byung-Gul Jun, Martin, Lee, Chi Hwan, 2023. In situ spray polymerization of conductive polymers for personalized E-textiles. ACS Nano 17, 22733–22743. https://pubs.acs.org/doi/10.1021/acsnano.3c07283.
- Chung, Ha Uk, Rwei, Alina Y., Hourlier-Fargette, Aurélie, Xu, Shuai, Lee, KunHyuck, Dunne, Emma C., Xie, Zhaoqian, Liu, Claire, Carlini, Andrea, Dong, Hyun Kim, Ryu, Dennis, Kulikova, Elena, Cao, Jingyue, Odland, Ian C., Fields, Kelsey B., Hopkins, Brad, Banks, Anthony, Ogle, Christopher, Grande, Dominic, Park, Jun Bin, Kim, Jongwon, Irie, Masahiro, Jang, Hokyung, Lee, JooHee, Park, Yerim, Kim, Jungwoo, Jo, Han Heul, Hahm, Hyoungjo, Avila, Raudel, Xu, Yeshou, Namkoong, Myeong, Kwak, Jean Won, Suen, Emily, Paulus, Max A., Kim, Robin J., Parsons, Blake V., Human, Kelia A., Kim, Seung Sik, Patel, Manish, Reuther, William, Kim, Hyun Soo, Lee, Sung Hoon, Leedle, John D., Yun, Yeojeong, Rigali, Sarah, Son, Taeyoung, Jung, Inhwa, Arafa, Hany, Soundararajan, Vinaya R., Ollech, Ayelet, Shukla, Avani, Allison, Bradley, Molly, Schau, Rand, Casey M., Marsillio, Lauren E., Harris, Zena L., Huang, Yonggang, Aaron, Hamvas, Paller, Amy S., Weese-Mayer, Debra E., Lee, Jong Yoon, Rogers, John A., 2020. Skin-interfaced biosensors for advanced wireless physiological monitoring in neonatal and pediatric intensive-care units. Nat. Med. 26, 418–429. https://doi.org/10.1038/s41591-020-0792-9.
- Couëtil, Laurent L., Rosenthal, Frank S., DeNicola, Dennis B., Chilcoat, Clayton D., 2001. Clinical signs, evaluation of bronchoalveolar lavage fluid, and assessment of pulmonary function in horses with inflammatory respiratory disease. Am. J. Vet. Res. 62, 538–546. https://doi.org/10.2460/ajvr.2001.62.538.
- Couetil, L., Hammer, J., Miskovic Feutz, M., Nogradi, N., Perez-Moreno, C., Ivester, K., 2012. Effects of N-butylscopolammonium bromide on lung function in horses with recurrent airway obstruction. J. Vet. Intern. Med. 26, 1433–1438. https://doi.org/ 10.1111/j.1939-1676.2012.00992.x.
- Couetil, Laurent, Cardwell, Jacqueline M., Leguillette, Renaud, Mazan, Melissa, Richard, Eric, Bienzle, Dorothee, Bullone, Michela, Gerber, Vinzenz, Ivester, Kathleen, Lavoie, Jean-Pierre, Martin, James, Gabriel, Moran, Niedźwiedź, Artur, Pusterla, Nicola, Swiderski, Cyprianna, 2020. Equine asthma: current understanding and future directions. Front. Vet. Sci. 7, 450. https://doi.org/10.3389/fvets.2020.00450.
- De Grauw, J.C., Van Loon, J.P.A.M., 2016. Systematic pain assessment in horses. Vet. J. 209, 14–22. https://doi.org/10.1016/j.tvjl.2015.07.030.
- de Lagarde, M., Rodrigues, N., Chevigny, M., Beauchamp, G., Albrecht, B., Lavoie, J.P., 2014. N-butylscopolammonium bromide causes fewer side effects than atropine when assessing bronchoconstriction reversibility in horses with heaves. Equine Vet. J. 46 (4), 474–478. https://doi.org/10.1111/evj.12229.
- Decloedt, A., Borowicz, H., Slowikowska, M., Chiers, K., van Loon, G., Niedzwiedz, A., 2017. Right ventricular function during acute exacerbation of severe equine asthma. Equine Vet. J. 49, 603–608. https://doi.org/10.1111/evj.12675.
- Fang, Yunsheng, Zou, Yongjiu, Xu, Jing, Chen, Guorui, Zhou, Yihao, Deng, Weili, Zhao, Xun, Roustaei, Mehrdad, Hsiai, Tzung K., Chen, Jun, 2021. Ambulatory

- cardiovascular monitoring via a machine-learning-assisted textile triboelectric sensor. Adv. Mater. 33, 2104178. https://doi.org/10.1002/adma.202104178.
- Gerber, V., Robinson, N.E., Luethi, S., Marti, E., Wampfler, B., Straub, R., 2003. Airway inflammation and mucus in two age groups of asymptomatic well-performing sport horses. Equine Vet. J. 35 (5), 491–495. https://doi.org/10.2746/042516403775600424.
- Gleerup, K.B., Lindegaard, C., 2015. Recognition and quantification of pain in horses: a tutorial review. Equine Vet. Educ. 28 (1), 47–57. https://doi.org/10.1111/ eve.12383.
- Hawkins, J.F., Couetil, L., Miller, M.A., 2014. Maintenance of arytenoid abduction following carbon dioxide laser debridement of the articular cartilage and joint capsule of the cricoarytenoid joint combined with prosthetic laryngoplasty in horses: an in vivo and in vitro study. Vet. J. 199, 275–280. https://doi.org/10.1016/j. tvjl.2013.11.027.
- Hotchkiss, J.W., Reid, S.W.J., Christley, R.M., 2010. A survey of horse owners in Great Britain regarding horses in their care. Part 2: risk factors for recurrent airway obstruction. Equine Vet. J. 39 (4), 301–308. https://doi.org/10.2746/ 042516407X180129
- Hu, Hongjie, Huang, Hao, Li, Mohan, Gao, Xiaoxiang, Yin, Lu, Qi, Ruixiang, Wu, Ray S., Chen, Xiangjun, Ma, Yuxiang, Shi, Keren, Li, Chenghai, Maus, Timothy M., Huang, Brady, Lu, Chengchangfeng, Lin, Muyang, Zhou, Sai, Lou, Zhiyuan, Gu, Yue, Chen, Yimu, Lei, Yusheng, Wang, Xinyu, Wang, Ruotao, Yue, Wentong, Yang, Xinyi, Bian, Yizhou, Mu, Jing, Park, Geonho, Xiang, Shu, Cai, Shengqiang, Corey, Paul W., Wang, Joseph, Xu, Sheng, 2023. A wearable cardiac ultrasound imager. Nature 613, 667–675. https://doi.org/10.1038/s41586-022-05498-z.
- Ivester, Kathleen M., Couëtil, Laurent L., Moore, George E., 2018. An observational study of environmental exposures, airway cytology, and performance in racing thoroughbreds. J. Vet. Intern. Med. 32, 1754–1762. https://doi.org/10.1111/ ivim.15226.
- Kee, Phoebe, Anderson, Neil, Gargiulo, Gaetano D., Velie, Brandon D., 2023. A synopsis of wearable commercially available biometric-monitoring devices and their potential applications during gallop racing. Equine Vet. Educ. 35 (10), 551–560. https://doi. org/10.1111/eye.13800
- Kim, Hyejung, Firat Yazicioglu, Refet, Merken, Patrick, Van Hoof, Chris, Yoo, Hoi-Jun, 2010. ECG signal compression and classification algorithm with quad level vector for ECG Holter system. IEEE Trans. Inf. Technol. Biomed. 14 (1), 93–100. https://doi.org/10.1109/TITB.2009.2031638.
- Kim, Johee, Yoo, Seonggwang, Liu, Claire, Kwak, Sung Soo, Walter, Jessica R., Xu, Shuai, Rogers, John A., 2023. Skin-interfaced wireless biosensors for perinatal and paediatric health. Nat. Rev. Bioeng. 1, 631–647. https://doi.org/10.1038/ s4422.023.0030000.0
- Kwak, Sung Soo, Yoo, Seonggwang, Avila, Raudel, Chung, Ha Uk, Jeong, Hyoyoung, Liu, Claire, Vogl, Jamie L., Kim, Joohee, Yoon, Hong-Joon, Park, Yoonseok, Ryu, Hanjun, Lee, Geumbee, Kim, Jihye, Koo, Jahyun, Oh, Yong Suk, Kim, Sungbong, Xu, Shuai, Zhao, Zichen, Xie, Zhaoqian, Huang, Yonggang, Rogers, John A., 2021. Skin-integrated devices with soft, Holey Architectures for wireless physiological monitoring, with applications in the neonatal intensive care unit. Adv. Mater. 33, e2103974. https://doi.org/10.1002/adma.202103974.
- Lee, Mina, Park, Taewoong, Kim, Chaemin, Park, Sung-Min, 2020. Characterization of a magneto-active membrane actuator comprising hard magnetic particles with varying crosslinking degrees. Mater. Des. 195, 108921. https://doi.org/10.1016/j.matdes.2020.108921.
- Leduc, Laurence, Leclère, Mathilde, Gauthier, Laurie Girardot, Marcil, Olivier, Lavoie, Jean-Pierre, 2024. Severe asthma in horses is associated with increased airway innervation. J. Vet. Intern. Med. 38, 485–494. https://doi.org/10.1111/ jvim.16941.
- Leroux, A.A., Detilleux, J., Sandersen, C.F., Borde, L., Houben, R.M.A.C., Al Haidar, A., Art, T., Amory, H., 2013. Prevalence and risk factors for cardiac diseases in a hospital-based population of 3,434 horses (1994-2011). J. Vet. Intern. Med. 27, 1563–1570. https://doi.org/10.1111/jvim.12197.
- 2019 Lorello, O., Ramseyer, A., Burger, D., Gerber, V., Navas de Solis, C., 2019. Cardiovascular variables in eventing and endurance horses over a season. J. Vet. Cardiol. 21, 67–78. https://doi.org/10.1016/j.jvc.2018.08.004.
- Luo, Yifei, Abidian, Mohammad Reza, Ahn, Jong-Hyun, Akinwande, Deji, Andrews, Anne M., Antonietti, Markus, Bao, Zhenan, Berggren, Magnus, Berkey, Christopher A. Bettinger, Christopher John, Chen, Jun, Chen, Peng, Cheng, Wenlong, Cheng, Xu, Choi, Seon-Jin, Chortos, Alex, Dagdeviren, Canan, Dauskardt, Reinhold H., Di, Chong-an, Dickey, Michael D., Duan, Xiangfeng, Facchetti, Antonio, Fan, Zhiyong, Fang, Yin, Feng, Jianyou, Feng, Xue, Gao, Huajian, Gao, Wei, Gong, Xiwen, Guo, Chuan Fei, Guo, Xiaojun, Hartel, Martin C., He, Zihan, Ho, John S., Hu, Youfan, Huang, Qiyao, Huang, Yu, Huo, Fengwei, Hussain, Muhammad M., Ali, Javey, Jeong, Unyong, Jiang, Chen, Jiang, Xingyu, Kang, Jiheong, Karnaushenko, Daniil, Ali, Khademhosseini, Kim, Dae-Hyeong, Kim, Il-Doo Kireev, Dmitry, Kong, Lingxuan, Lee, Chengkuo, Lee, Nae-Eung, Lee, Pooi See, Lee, Tae-Woo, Li, Fengyu, Li, Jinxing, Liang, Cuiyuan, Lim, Chwee Teck, Lin, Yuanjing, Lipomi, Darren J., Liu, Jia, Liu, Kai, Liu, Nan, Liu, Ren, Liu, Yuxin, Liu, Yuxuan, Liu, Zhiyuan, Liu, Zhuangjian, Loh, Xian Jun, Lu, Nanshu, Lv, Zhisheng, Magdassi, Shlomo, Malliaras, George G., Matsuhisa, Naoji, Nathan, Arokia, Niu, Simiao, Pan, Jieming, Pang, Changhyun, Pei, Qibing, Peng, Huisheng, Qi, Dianpeng, Ren, Huaying, Rogers, John A., Rowe, Aaron, Schmidt, Oliver G., Sekitani, Tsuyoshi, Seo, Dae-Gyo, Shen, Guozhen, Xing, Sheng, Shi, Qiongfeng, Someya, Takao, Song, Yanlin, Stavrinidou, Eleni, Su, Meng, Sun, Xuemei, Takei, Kuniharu, Tao, Xiao-Ming, Tee, Benjamin C.K., Thean, Aaron Voon-Yew, Trung, Tran Quang, Wan, Changjin, Wang, Huiliang, Wang, Joseph, Wang, Ming, Wang, Sihong, Wang, Ting, Zhong, Lin Wang, Weiss, Paul S., Wen, Hanqi, Xu, Sheng, Xu, Tailin, Yan, Hongping, Yan, Xuzhou, Yang, Hui, Yang, Le, Yang, Shuaijian,

- Yin, Lan, Yu, Cunjiang, Yu, Guihua, Yu, Jing, Yu, Shu-Hong, Yu, Xinge, Zamburg, Evgeny, Zhang, Haixia, Zhang, Xiangyu, Zhang, Xiaosheng, Zhang, Xueji, Zhang, Yihui, Zhang, Yu, Zhao, Siyuan, Zhao, Xuanhe, Zheng, Yuanjin, Zheng, YuQing, Zheng, Zijian, Zhou, Tao, Zhu, Bowen, Zhu, Ming, Zhu, Rong, Zhu, Yangzhi, Zhu, Yong, Zou, Guijin, Chen, Xiaodong, 2023. Technology roadmap for flexible sensors. ACS Nano 17, 5211–5295. https://doi.org/10.1021/acsnano.2c12606.
- Marlin, D.J., Schrotert, R.C., Cashman, P.M.M., Deaton, C.M., Poole, D.C., Kindig, C.A., McDonough, P., Erickson, H.H., 2002. Movements of thoracic and abdominal compartments during ventilation at rest and during exercise. Equine Vet. J. 34 (S34), 384–390. https://doi.org/10.1111/j.2042-3306.2002.tb05453.x.
- Meng, Keyu, Liu, Zixiao, Xiao, Xiao, Manshaii, Farid, Li, Pei, Yin, Junyi, Wang, Haiyan, Mei, Haixia, Sun, Yubo, He, Ximin, Yang, Jun, Chen, Jun, 2024. Bioinspired wearable pulse sensors for ambulant cardiovascular monitoring and biometric authentication. Adv. Funct. Mater. 34, 2403163. https://doi.org/10.1002/adfm.202403163.
- Min, Jihong, Tu, Jiaobing, Xu, Changhao, Lukas, Heather, Shin, Soyoung, Yang, Yiran, Solomon, Samuel A., Mukasa, Daniel, Gao, Wei, 2023. Skin-interfaced wearable sweat sensors for precision medicine. Chem. Rev. 123, 5049–5138. https://doi.org/10.1021/acs.chemrev.2c00823
- Mitchell, Katharyn J., 2019. Equine electrocardiography. Vet. Clin. N. Am. Equine Pract. 35, 65–83. https://doi.org/10.1016/j.cveq.2018.12.007.
- Mitchell, Katharyn J., Schwarzwald, Colin C., Bevevino, Kari, Cristobal, Navas de Solis, 2020. Science-in-brief: Equine cardiology virtual retreat June 2020. Equine Vet. J. 52, 787–789. https://doi.org/10.1111/evj.13335.
- Mitchell, Katharyn J., Schwarzwald, Colin C., 2021. Heart rate variability analysis in horses for the diagnosis of arrhythmias. Vet. J. 268, 105590. https://doi.org/
- Mohapatra, Payal, Aravind, Vasudev, Bisram, Marisa, Lee, Young-Joong, Jeong, Hyoyoung, Jinkins, Katherine, Gardner, Richard, Streamer, Jill, Bowers, Brent, Cavuoto, Lora, Banks, Anthony, Xu, Shuai, Rogers, John, Cao, Jian, Qi, Zhu, Guo, Ping, 2024. Wearable network for multilevel physical fatigue prediction in manufacturing workers. PNAS Nexus 3, pgae421. https://doi.org/10.1093/pnasnexus/pgae421.
- Vives, Berta Mozo, Mainguy-Seers, Sophie, Lavoie, Jean-Pierre, 2024. Comparative study of the bronchodilator efficacy and adverse effects of salbutamol and hyoscine butylbromide in horses with severe asthma. J. Vet. Intern. Med. 38, 1835–1841. https://doi.org/10.1111/jvim.17057.
- Navas de Solis, Cristobal Navas, Gabbett, Tim, King, Melissa R., Keene, Robert, McKenzie, Erica, 2022. Science in brief: the Dorothy Havemeyer International Workshop on poor performance in horses: recent advances in technology to improve monitoring and quantification. Equine Vet. J. 54, 844–846. https://doi.org/10.1111/evi.13608.
- Navas de Solis, Cristobal Navas, Solomon, Claire, Durando, Mary, Stefanovski, Darko, 2024. Electrocardiograms from different types of exercise in eventing horses with and without cardiac signs. Equine Vet. J. 1–10. https://doi.org/10.1111/evj.14449.
- Navas de Solis, C., 2019. Cardiovascular response to exercise and training, exercise testing in horses. Vet. Clin. N. Am. Equine Pract. 35 (1), 159–173. https://doi.org/ 10.1016/j.cyeq.2018.11.003.

- Pan, Yuxiang, Su, Xiaoyu, Liu, Ying, Fan, Peidi, Li, Xunjia, Ying, Yibin, Jianfeng, Ping, 2024. A laser-engraved wearable electrochemical sensing patch for heat stress precise individual management of horse. Adv. Sci. 11, e2310069. https://doi.org/10.1002/advs.202310069.
- Park, Taewoong, Mahmud, Talha Ibn, Lee, Junsang, Hong, Seokkyoon, Park, Jae Young, Ji, Yuhyun, Chang, Taehoo, Yi, Jonghun, Kim, Min Ku, Patel, Rita R., Kim, Dong Rip, Kim, Young L., Lee, Hyowon, Zhu, Fengqing, Lee, Chi Hwan, 2024. A machine-learning-enabled smart neckband for monitoring dietary intake. PNAS Nexus 3, pgae156. https://doi.org/10.1093/pnasnexus/pgae156.
- Petsche, Vicki M., Derksen, Frederik J., Edward Robinson, N., 1994. Tidal breathing flow-volume loops in horses with recurrent airway obstruction (heaves). Am. J. Vet. Res. 55 (7), 885–891. https://doi.org/10.2460/ajvr.1994.55.07.885.
- Ray, Tyler R., Choi, Jungil, Bandodkar, Amay J., Krishnan, Siddharth, Philipp, Gutruf, Tian, Limei, Ghaffari, Roozbeh, Rogers, John A., 2019. Bio-integrated wearable systems: a comprehensive review. Chem. Rev. 119, 5461–5533. https://doi.org/ 10.1021/acs.chemrev.8b00573.
- Scott, Brett D., Martin, Mike, 2020. Understanding vital life signs in horses. https://t exashelp.tamu.edu/wp-content/uploads/2016/02/understanding-vital-life-signsin-horses.pdf. (Accessed 26 September 2025).
- Sani, Ehsan Shirzaei, Xu, Changhao, Wang, Canran, Song, Yu, Min, Jihong, Tu, Jiaobing, Solomon, Samuel A., Li, Jiahong, Banks, Jaminelli L., Armstrong, David G., Gao, Wei, 2023. A stretchable wireless wearable bioelectronic system for multiplexed monitoring and combination treatment of infected chronic wounds. Sci. Adv. 9, eadf7388. https://doi.org/10.1126/sciadv.adf7388.
- Song, Yu, Min, Jihong, Yu, You, Wang, Haobin, Yang, Yiran, Zhang, Haixia, Gao, Wei, 2020. Wireless battery-free wearable sweat sensor powered by human motion. Sci. Adv. 6, eaay9842. https://doi.org/10.1126/sciadv.aay9842.
- Vadrevu, Simhadri, Sabarimalai Manikandan, M., 2019. A Robust pulse onset and peak detection method for automated PPG signal analysis system. IEEE Trans. Instrum. Meas. 68 (3), 807–817. https://doi.org/10.1109/TIM.2018.2857878.
- Verheyen, T., Decloedt, A., De Clercq, D., Deprez, P., Sys, S.U., van Loon, G., 2010. Electrocardiography in horses-part 1: how to make a good recording. Vlaams Diergen. Tijds. 79. https://doi.org/10.21825/vdt.87463.
- Wang, Chunfeng, Wang, Chonghe, Huang, Zhenlong, Xu, Sheng, 2018. Materials and structures toward soft electronics. Adv. Mater. 30, e1801368. https://doi.org/ 10.1002/adma.201801368.
- Wang, Minqiang, Yang, Yiran, Min, Jihong, Song, Yu, Tu, Jiaobing, Mukasa, Daniel, Ye, Cui, Xu, Changhao, Heflin, Nicole, McCune, Jeannine S., Hsiai, Tzung K., Li, Zhaoping, Gao, Wei, 2022. A wearable electrochemical biosensor for the monitoring of metabolites and nutrients. Nat. Biomed. Eng. 6, 1225–1235. https://doi.org/10.1038/s41551-022-00916-z.
- Xu, Shuai, Kim, Joohee, Walter, Jessica R., Ghaffari, Roozbeh, Rogers, John A., 2022. Translational gaps and opportunities for medical wearables in digital health. Sci. Transl. Med. 14, eabn6036. https://doi.org/10.1126/scitranslmed.abn6036.
- Yin, Junyi, Wang, Shaolei, Tat, Trinny, Chen, Jun, 2024. Motion artefact management for soft bioelectronics. Nat. Rev. Bioeng. 2, 541–558. https://doi.org/10.1038/ s44222-024-00175-4.